Transp Porous Med (2008) 71:233–251
DOI 10.1007/s11242-007-9123-6

The transverse permeability of disordered fiber arrays: a statistical correlation in terms of the mean nearest interfiber spacing

Xiaoming Chen · Thanasis D. Papathanasiou

Received: 13 June 2006 / Accepted: 9 March 2007 / Published online: 18 April 2007

Abstract In the porous media literature, unidirectional fibrous systems are broadly categorized as ordered or disordered. The former class, easily tractable for analysis purposes but limited in its relation to reality, involves square, hexagonal and various staggered arrays. The latter class involves everything else. While the dimensionless hydraulic permeability of ordered fibrous media is known to be a deterministic function of their porosity ϕ, the parameters affecting the permeability of disordered fiber arrays are not very well understood. The objective of this study is to computationally investigate flow across many unidirectional arrays of randomly placed fibers and derive a correlation between K and some measure of their microstructure. In the process, we explain the wide scatter in permeability values observed computationally as well as experimentally. This task is achieved using a parallel implementation of the Boundary Element Method (BEM). Over 600 simulations are carried out in two-dimensional geometries consisting of 576 fiber cross-sections placed within a square unit cell by a Monte Carlo procedure. The porosity varies from 0.45 to 0.90. The computed permeabilities are compared with earlier theoretical results and experimental data. Analysis of the computational results reveals that the permeability of disordered arrays with $\phi < 0.7$ is reduced as the non-uniformity of the fiber distribution increases. This reduction can be substantial at low porosities. The key finding of this study is a direct correlation between K and the mean nearest inter-fiber spacing $\bar{\delta}_1$, the latter depending on the microstructure of the fibrous medium.

Keywords Permeability · Fibrous media · Boundary element method · Liquid molding

X. Chen · T. D. Papathanasiou (✉)
Department of Chemical Engineering, University of South Carolina, Columbia, SC 29208, USA
e-mail: papathan@engr.sc.edu

1 Introduction

Viscous flow through fibrous media is a problem of long-standing interest in engineering due to its importance in the manufacturing and process industries. With specific reference to manufacturing, flow through fibrous media is of direct relevance to several composites forming operations such as liquid molding, pultrusion, and autoclave processing. Under creeping flow conditions, the flow of a resin through a fibrous preform can be macroscopically described by Darcy's law:

$$\bar{\mathbf{u}} = -\frac{\mathbf{K}}{\mu} \cdot \nabla p \tag{1}$$

which is a linear relationship between the local superficial fluid velocity $\bar{\mathbf{u}}$ and the local pressure gradient ∇p. In Eq. 1 the permeability tensor $\mathbf{K}$ is a property characteristic of the porous medium. In a mold filling simulation Eq. 1 is combined with the continuity equation for steady-state incompressible flow ($\nabla \cdot \bar{\mathbf{u}} = 0$) to yield an elliptic differential equation for pressure:

$$\nabla \cdot \left(\frac{\mathbf{K}}{\mu} \cdot \nabla p \right) = 0. \tag{2}$$

To numerically solve Eq. 2, nodal permeability values must be specified at points dictated by the domain discretization method; the accuracy of these nodal values evidently affects the outcome of simulation. For this purpose, permeability measurement techniques suitable for fibrous media similar to those used in liquid molding (preforms) have been developed (Ferland et al. 1996; Gebart and Lidstrom 1996; Parnas et al. 1997; Weitzenbock et al. 1999; Lundstrom et al. 1999). However, these measurements are subject to large uncertainties, mainly caused by structural variations and/or deformation of the preform during the experiment. Therefore, in parallel with the development of more accurate and faster permeability testing methods, a great deal of effort has been devoted to developing models that would predict the permeability of a fibrous preform based on knowledge of its structure. Several studies have appeared in recent years, in which the permeability of fibrous preforms was sought as function of the geometry of the interstitial space between fiber tows (Nordlund et al. 2006; Ngo and Tamma 2004; Song et al. 2004; Loendersloot et al. 2004; Yu et al. 2002). The effect on K of the distortions introduced by the stitching process in otherwise unidirectional plies of fibers was addressed using a network model that accounted for the statistical distribution of the flow channels opened by the stitching process (Loendersloot et al. 2004). The fractal nature of the interstitial spaces of a fibrous perform was accounted for in a model for the in-plane permeability of fabrics developed by Yu et al. (2002); good agreement with experimental data was found. The works mentioned above allow for sophisticated description of the interstitial space; however, they ignore the flow within the fiber bundles themselves. Because of the focus at the mm-scale region typically associated with the interstitial space between fiber bundles, these results are of no direct applicability to the particular problem we consider here, namely transverse flow through unidirectional fiber arrays. This type of flow would occur within fiber bundles in a preform during mold filling. It would also characterize flow in more general fibrous media (for example fibrous reactors, filters etc.), in which fibers are not utilized in the form of bundles. Analysis of flow through such systems is not a new problem. In early studies, unidirectional fibrous media were typically idealized as periodic (square or hexagonal) arrays

of cylinders, and analytical as well as numerical solutions expressing the dimensionless permeabity K/R^2 , where (R) is the fiber radius, as a function of ϕ, have been obtained (Happel 1959; Hasimoto 1959; Keller 1964; Gebart 1992; Sangani and Acrivos 1982; Drummond and Tahir 1984; Skartsis et al. 1992a; Bruschke and Advani 1993; Howells 1974; Spielman and Goren 1968; Koch and Brady 1986; Sangani and Yao 1988; Ghaddar 1995). Random fiber arrays are, in principle, well-suited for analysis using effective medium approaches. Work in this area (Howells 1974; Spielman and Goren 1968; Koch and Brady 1986) has produced results that are valid at the dilute (high porosity, $\phi \rightarrow 1$) limit but questionable in the porosity range of interest to composites manufacturing, e.g., $\phi \leq 0.6$. Application of some of the above results (Happel 1959; Hasimoto 1959; Keller 1964; Gebart 1992; Sangani and Acrivos 1982; Drummond and Tahir 1984; Skartsis et al. 1992b; Bruschke and Advani 1993) in the area of composites manufacturing has been reviewed by Skartsis et al. (1992a) and Astrom et al. (1992).

Large discrepancies are frequently observed between theoretical results and experimental data obtained in real fiber beds. A notable feature of experimental data obtained in the latter is the substantial scatter in the measured values of K. It has been widely assumed that these discrepancies are caused by the non-uniformity of real fiber beds (Parnas et al. 1997; Skartsis et al. 1992a; Astrom et al. 1992). Indeed, fiber packing disorder and fiber size variations are typical in fiber preforms. Hence, it is not unreasonable that a function of porosity alone will not be sufficient to explain the observed variability in permeability data. In recent years, several authors have investigated, either analytically or numerically, the effects of fiber size variation, perturbed fiber positions, and fiber lattice imperfections on the transverse permeability of unidirectional fiber arrays (Sangani and Yao 1988; Cai and Berdichevsky 1993; Lundstrom and Gebart 1995; Papathanasiou and Lee 1997; Papathanasiou 2001). Of particular interest to our study are the works of Sangani and Yao (1988) and Lundstrom and Gebart (1995). Sangani and Yao (1988) used a multipole collocation method to numerically solve the equations of Stokes flow across random fiber arrays. CPU speed and memory storage limitations allowed systems consisting of no more than 25 fibers to be considered. Mean permeability values were obtained by averaging results over a number of different configurations. Sangani and Yao (1988) observed significant scatter in the permeability values obtained in random fiber arrays and reached the conclusion that some measure of microstructure should be included in models for the permeability of random fiber arrays. They did not report any such analysis of their computational results. Lundstrom and Gebart (1995) developed analytical models for the permeability of several types of "perturbed" fiber arrays based on the lubrication approximation. Their models were compared to numerical results by Papathanasiou (2001) and their predictions were found in very good agreement with simulation for a wide range of the pertinent parameters. One feature of the model of Lundstrom and Gebart (1995), that is of particular interest to the present study, is its ability to incorporate a varying inter-fiber spacing at a given fiber volume fraction; as such it offers the opportunity to examine the effect of inter-fiber spacing on permeability from a theoretical perspective. These models, as they relate to the present study, are discussed in Appendix 1.

In this work we adopt a direct numerical approach using the Boundary Element Method (BEM). A parallel version of the BEM has been implemented in order to overcome the difficulties associated with CPU time and memory storage requirements. A large number of simulations in large unit cells, each containing 576 fibers, with varied porosity and varied degrees of local fiber aggregation, were carried out.

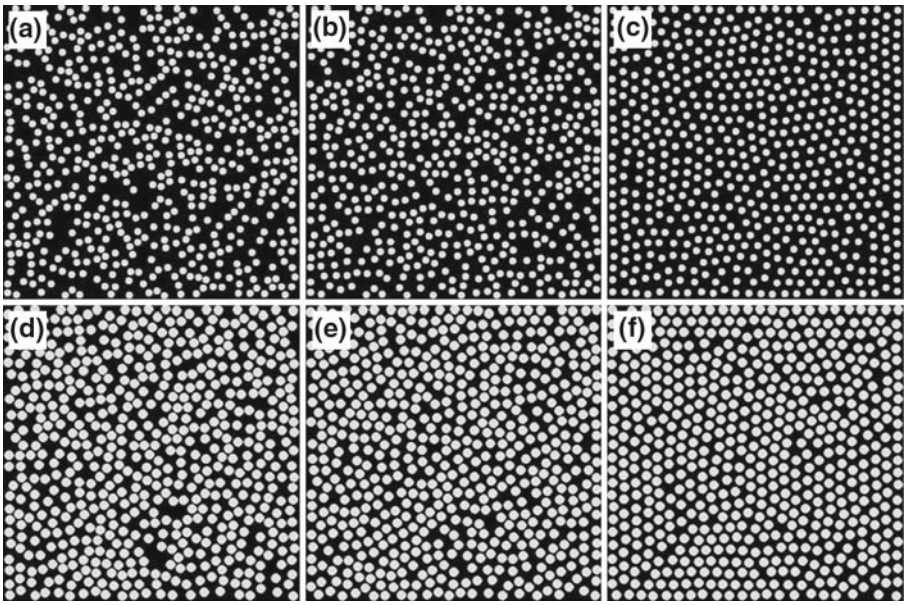

Fig. 1 Fiber distributions generated by a Monte Carlo procedure, each with 576 fibers: (**a**) $\phi = 0.7, \delta_{\min} = 0.1R$; (**b**) $\phi = 0.7, \delta_{\min} = 0.4R$; (**c**) $\phi = 0.7, \delta_{\min} = 1.0R$; (**d**) $\phi = 0.5, \delta_{\min} = 0.1R$; (**e**) $\phi = 0.7, \delta_{\min} = 0.2R$; (**f**) $\phi = 0.5, \delta_{\min} = 0.4R$

The spatial statistics of the fiber distributions in terms of the mean nearest inter-fiber distance were quantified. In the following, the problem formulation is given in Sect. 2. This is followed by Sect. 3 for a description of the fiber distributions. In Sect. 4, we investigate the effect of the size of the unit cell on the computed permeability, compare our results with existing theoretical and experimental results, and finally develop a correlation between the permeability and the mean nearest inter-fiber spacing.

2 Problem formulation

We consider a fibrous medium composed of long cylindrical fibers with their axes oriented perpendicular to the direction of bulk flow. The computational unit cell represents a plane cut normal to the fibers' axes. As our focus is on the effect of the spatial distribution of fibers, these are of the same size; however, size variation can easily be incorporated in a numerical approach. Typical geometries are shown in Fig. 1. The method used for their generation is discussed in Sect. 3.1 below.

2.1 Governing equations

The governing equations for two-dimensional creeping flow in the inter-fiber space are:

$$\nabla \cdot \mathbf{u} = 0 \quad \text{on } \Omega \tag{3}$$

$$\mu \nabla^2 \mathbf{u} = \nabla p \quad \text{on } \Omega \tag{4}$$

Here $\mathbf{u}, p, \mu$, and Ω denote the velocity vector, pressure, viscosity, and the 2-D flow domain, respectively. With reference to Fig. 1, the bulk flow is assumed to occur from left to right. Symmetry conditions are applied to the boundaries parallel to the flow direction so that no flow will cross these boundaries. On the boundaries normal to the bulk flow direction, homogeneous pressures are specified and a pressure drop (Δp) is maintained between the two vertical boundary planes. The boundary conditions, in terms of tractions and velocities, are:

$$t_x = 0 \quad u_y = 0 \quad \text{at } y = 0,\ y = H \tag{5}$$

$$t_x = \Delta p \quad u_y = 0 \quad \text{at } x = 0 \tag{6}$$

$$t_x = 0 \quad u_y = 0 \quad \text{at } x = L \tag{7}$$

$$u_x = 0 \quad u_y = 0 \quad \text{on } \Gamma_f \tag{8}$$

where t_x is the traction component in the x direction and Γ_f denotes the fiber surface. Equation 8 specifies that no-slip boundary conditions are imposed on the fiber surfaces. Once the boundary solution is obtained by solving the pertinent equations, the flowrate Q in the bulk flow direction can be obtained by integrating the velocity profiles on the inflow or outflow boundary (of height H and length L in Fig. 1). The effective permeability K can then be calculated from Darcy's law as $K = Q\mu L/H\Delta p$. This is rendered dimensionless by dividing with the square of the fiber radius; it is this dimensionless permeability K/R^2 that is reported and discussed in the remainder of the manuscript.

2.2 Numerical method and parallelization

The governing equations can be cast into boundary integral representations involving boundary velocities and tractions only. This technique is well-established (Beer 2001; Gao and Davies 2002; Pozridikis 1992). Using fundamental solutions, the boundary integral equations are usually written as:

$$c_{ij}(x_p)u_j(x_p) = \int_\Gamma u^*_{ij}(x_q, x_p)t_j(x_q)d\Gamma - \int_\Gamma t^*_{ij}(x_q, x_p)u_j(x_q)d\Gamma, \tag{9}$$

where u^*_{ij} is the Stokeslet representing the fluid velocity at $\boldsymbol{x_p}$ in the ith direction due to a point force at $\boldsymbol{x_q}$ in the jth direction and t^*_{ij} is the corresponding fundamental solution for tractions. Isoparametric quadratic elements were used to discretize Eq. 9, providing second-order approximations for both geometry and field variables. After discretization, the resulting system of linear equations is usually represented as $[\mathbf{H}]\{\mathbf{u}\} = [\mathbf{G}]\{\mathbf{t}\}$, where $\{\mathbf{u}\}$ and $\{\mathbf{t}\}$ contain two complete sets of both known and unknown nodal velocity and tractions, respectively, and $[\mathbf{H}]$ and $[\mathbf{G}]$ are influence coefficient matrices whose elements are either non-singular, weakly-singular or singular integrals. The non-singular integrals were typically evaluated by 10-point Gaussian quadrature. The singular integrals were worked around by the well-known assumption of rigid-body motion, and the weakly singular integrals were evaluated by Gauss–Laguerre quadrature with the aid of coordinate transformation (cf. Gao and Davies 2002). To prevent the deterioration of accuracy of numerical quadrature in non-singular integrals, the ratio of the closest distance between two nodes at different elements to the element size should be kept above a certain value. In the worst case,

the closest distance between two nodes at different elements is equal to the minimum nearest inter-fiber spacing $\delta_{\min}$. Therefore, the discretization of fiber surfaces should be finer when $\delta_{\min}$ gets smaller. In this study, the smallest value of $\delta_{\min}$ is one-tenth of the fiber radius (R). We typically used 24–36 nodes per fiber. According to an error estimate proposed by Gao and Davis (2002), the distance-to-element ratio ($\frac{\delta_{\min}}{L_e}$) for a desired tolerance (ε_t) should be $\frac{\delta_{\min}}{L_e} = \frac{8}{3}[-10N_G/p_1 \ln(\varepsilon_t/2) - 1]^{3/4}$ where N_G is the order of the Gaussian quadrature used and p_1 is related to the order of the singularity (p) as $p_1 = \sqrt{2p/3 + 1}$. For example, for a tolerance $\varepsilon_t < 10^{-6}$ and a first order singularity, it should be $\delta_{\min}/L_e > 0.26$. It was observed that further refinement did not change the results significantly.

The inherent shortcoming of the BEM is that it results in dense and non-symmetric coefficient matrices. For large-scale problems, the solution of this dense linear system is the most time-consuming part in the BEM (scales with N_m^3, N_m being the size of the system matrix), an additional bottleneck being the Random Access Memory (RAM) that can be used. These difficulties can be partly overcome by utilizing distributed memory parallel computers, which offer expanded RAM as well as computing speedup. For this purpose, we developed an in-house parallel boundary element code with function calls to ScaLAPACK (Blackford et al. 1997) and MPI (Gropp and Lusk 1994) libraries. The coarse parallelism inherent to the matrix assembly, solution, and post-processing phases of the BEM was exploited when implementing the parallel code and the computing tasks were divided element-wise among the computing nodes. In the solution phase, the parallel L–U decomposition algorithm in ScaLAPACK (Blackford et al. 1997) and the associated two-dimensional block-cyclic data-decomposition scheme were adopted in order to improve parallel efficiency. The code was originally developed on an 8-node Microway Alpha cluster and latter was ported to run on an IBM Netfinity 4500R cluster with 256 nodes.

3 RVE construction and characterization

3.1 RVE construction

The RVEs considered by this study were constructed to represent a spectrum of disordered fiber distributions with varied degrees of heterogeneity. They were generated using a Monte Carlo (MC) procedure, which is similar to the method for generating an equilibrium ensemble of hard disks (Torquato 2002). The MC process starts with an initial fiber packing (square array in our case), then proceeds by randomly and sequentially perturbing each fiber's location. This is done by displacing the coordinates of the centroid of each fiber along each axis by amounts randomly and uniformly distributed in the interval $[-\Delta, \Delta]$, where Δ is the maximum allowable displacement amount. Starting from a square fiber lattice limits the value of Δ that can be used; that is Δ has to be smaller than the inter-fiber spacing corresponding to the square array. If, in its new location, a fiber neither overlaps with other fibers nor the RVE boundaries, this new location is accepted; otherwise it is rejected. The criterion used to test for overlapping is that the distance between two fiber surfaces is less than $\delta_{\min}$, and the distance between the fiber surface and the RVE boundaries is less than $\delta_{\min}/2$, where $\delta_{\min}$ is a parameter specified by the user. A cycle is completed

when all fibers have completed an attempted move, irrespective of whether this move was accepted or rejected. The microstructures generated in this manner are primarily governed by their porosity ϕ and the choice of the minimum allowable inter-fiber distance $\delta_{\min}$. In addition to this constraint, the RVE boundaries act like rigid walls keeping fibers from exiting the RVE. Typical fiber distributions are presented in Fig. 1 for different combinations of ϕ and $\delta_{\min}$. It is evident that small values of $\delta_{\min}$ result in patterns showing local (small scale) fiber aggregation while large values of $\delta_{\min}$ lead to more or less uniform distributions that show rather small deviations from a hexagonal lattice. The effect of $\delta_{\min}$ on fiber aggregation is more pronounced when ϕ is large. By varying $\delta_{\min}$, a spectrum of fiber distributions can be generated at the same porosity level, ranging from locally aggregated to homogeneous. For the fiber distributions generated at all porosity levels, the limiting value of $\delta_{\min}$ was taken as $0.1R$. This decision was made mainly out of numerical concerns as discussed in Sect. 2.2 above. In spite of this artificiality, we found that the resulting fiber distributions appear similar to the ones we observe in several liquid molded or pultruded unidirectional composites. The high end of $\delta_{\min}$ is limited by the spacing of a square fiber array.

3.2 Statistical descriptors

As our objective is to discriminate between various *random* fiber arrangements and to describe the permeability of such arrangements as a function of other parameters beyond porosity, the microstructure of such fiber arrangements needs to be properly quantified. There are several statistical descriptors that are useful for this purpose. One descriptor, namely the Ripley's $K_r(r)$ function (Ripley 1981), can be used to differentiate between regular, Completely Spatially Random (CSR), and clustered point patterns. For a set of points, this function is defined as:

$$K_r(r) = \frac{A}{N^2} \sum_{k=1}^{N} \frac{I_k(r)}{w_k(r)} \tag{10}$$

where $I_k(r)$ is the number of points found within distance r of an arbitrary point k, N is the total number of points in the area of interest A, and $w_k(r)$ is a correction factor taking account of the fact that it is possible that only a part of the observation area πr^2 falls within the area of interest A. $K_r(r)$ describes characteristics of point patterns at many length scales. The K_r-function of a Poisson distribution is $K_r(r) = \pi r^2$ and draws a dividing line between an inhibited or regular pattern and a clustered pattern. Estimates of $K_r(r)$ are expected to be smaller than πr^2 if the points form an inhibited or regular pattern, and to be larger than πr^2 in the presence of clustering or heterogeneity (Pyrz 1994; Diggle 2003). Furthermore, the extent of the deviation of $K_r(r)$ from πr^2 and the length scale at which such deviations occur give some additional insight into a microstructure. The L-plot, a linearized plot of $K_r(r)$ defined as: $L(r) = \sqrt{K_r(r)/\pi}$, is frequently used to show these deviations and the length scales at which they occur. The L-plot of a Poisson distribution is simply a straight line of 45-degree slope through the origin. In Fig. 3, we apply Ripley's K-function to characterize the fiber distributions given in Fig. 1. It is clear that at large distances all fiber distributions approach CSR and that significant deviations from CSR occur only at small length scales. This suggests that the fiber distributions are better distinguished by their small-scale features. It is also concluded that the fiber distributions considered

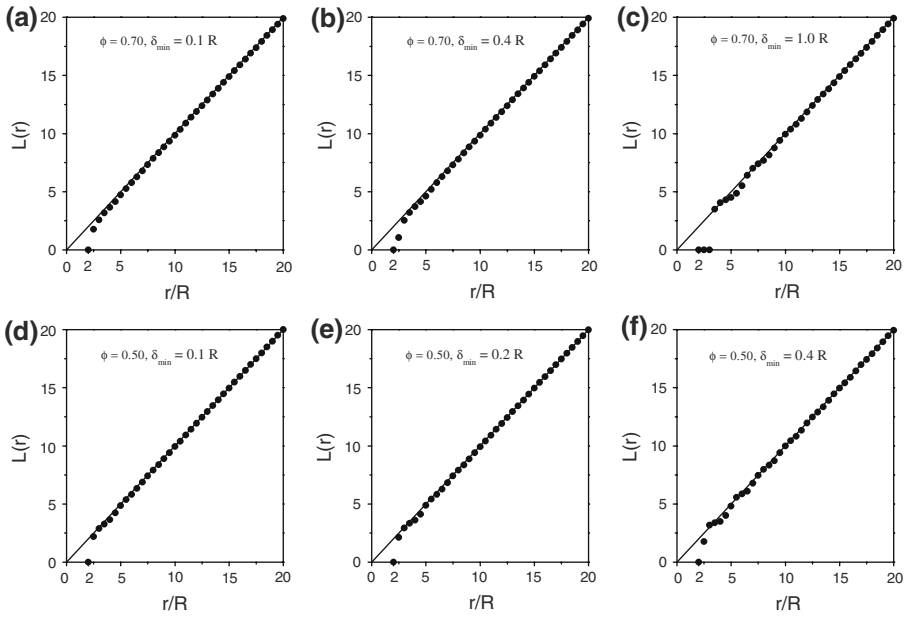

Fig. 2 $L(r)$ statistics for the fiber distributions shown in Fig. 1

by this study belong to the "regular" category (Torquato 2002; Diggle 2003). This is not a surprise as the non-zero physical dimension of a fiber makes the MC process essentially a self-inhibiting one.

Another useful statistical descriptor based on local information is the mean nearest neighbor distance $\bar{d}_1$. For each fiber k one can find a number of "neighbors", which are assigned with a subscript (i) in such a way that the nearest one corresponds to $i = 1$ and the others are in ascending order according to relative distances. These center-to-center distances are denoted as $\{d_i^{(k)}\}$. The nearest neighbor distance for a reference fiber k is therefore the minimum in this distance set, i.e., $d_1^{(k)} = \min\{d_i^{(k)}\}$. For a population of fibers, the mean nearest neighbor distance, denoted as $\bar{d}_1$, is simply the arithmetic mean of the set $d_1^{(k)}$. This metric is frequently used to indicate the degree of local heterogeneity in spatial point patterns (Ripley 1981; Diggle 2003). Small values of $\bar{d}_1$ are associated with disordered patterns, while large $\bar{d}_1$ indicate a homogeneous arrangement. By subtracting the fiber diameter D, $d_1^{(k)}$ is translated to $\delta_1^{(k)}$, which is the closest spacing between the k^{th} reference fiber and its neighbors. Because δ_1 takes explicit account of the fluid space between two fibers, we will use δ_1 in the rest of this paper. We will also refer to the arithmetic mean of $\left\{\delta_1^{(k)}\right\}$ $(k = 1, \ldots, N_\text{f})$ as the mean nearest inter-fiber spacing, denoted as $\bar{\delta}_1$. With reference to Fig. 1, the statistics of δ_1 for various arrays are shown in Fig. 2. These are fitted to the Weibull distribution function:

$$F(\delta_1) = 1 - \exp\left[-\lambda\,(\delta_1 - \gamma)^\beta\right], \tag{11}$$

where λ, γ, and β are the shape, location, and slope parameters, respectively. The estimated values for λ, γ, and β are given in Table 1. Note that γ is equivalent to δ_min.

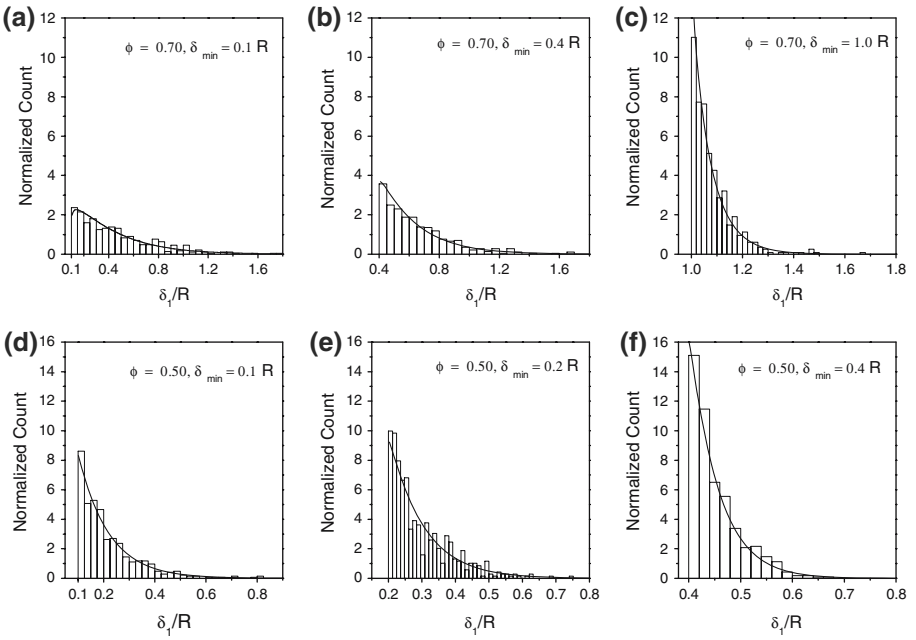

Fig. 3 Histograms of δ_1 for the fiber distributions shown in Fig. 1 and the corresponding non-linear fit as of Eq. 11. The normalized count on the Y-axis is the number of counts in the bin class divided by the total number of counts times the bin class width

Table 1 Parameter fitting according to Eq. 11 for the distributions δ_1 shown in Fig. 1a–e

Case	γ	β	λ	COD	$\gamma+1/\lambda$	$\bar{\delta}_1$
(a)	0.1	1.090 ± 0.014	3.052 ± 0.072	0.997	0.428	0.450
(b)	0.4	1.030 ± 0.013	4.255 ± 0.077	0.997	0.635	0.649
(c)	1.0	0.957 ± 0.009	12.07 ± 0.271	0.998	1.082	1.080
(d)	0.1	1.003 ± 0.008	8.560 ± 0.105	0.999	0.217	0.216
(e)	0.2	1.016 ± 0.023	10.28 ± 0.373	0.997	0.297	0.295
(f)	0.4	1.030 ± 0.012	20.01 ± 0.526	0.999	0.450	0.454

COD stands for coefficient of determination

It is also noticed that all the estimated β values are around one, implying the distributions of δ_1 are essentially exponential distributions. For an exponential distribution, its population mean is estimated as $\gamma + 1/\lambda$. Comparing the last two columns of Table 1, it can be seen that $\bar{\delta}_1$, as calculated from the exponential distributions, are reasonably close to $\bar{\delta}_1$ based on arithmetic averaging. It is known that at the same porosity level, $\bar{\delta}_1$ for a more uniform fiber distribution is greater than that for a non-uniform distribution (Ripley 1981; Diggle 2003).

4 Results and discussion

4.1 RVE size

The stochastic nature of the fiber distribution leads to scatter in the computed permeability data. In this study, a number (N_r) of random realizations was generated for

Table 2 Numerical simulation settings

ϕ	$\delta_{\min}/R$	N_f	N_r
0.45	0.10, 0.20, 0.30	576	20
0.50	0.10,0.20, 0.30, 0.40	576	20
0.60	0.10,0.20,0.30, 0.40, 0.60,0.75	576	20
0.70	0.10,0.20,0.30, 0.40, 0.60, 0.80, 0.90	576	20
0.80	0.10,0.20,0.40, 0.60, 0.80, 1.00, 1.20	576	20
0.90	0.10,0.30, 1.00, 1.50	576	20

each class of fiber distributions (characterized by ϕ and $\bar{\delta}_1$) and the permeability values were computed for the resulting unit cells. The average dimensionless permeability and its standard deviation are then calculated as:

$$\langle K \rangle = \frac{1}{N_{\mathrm{r}}} \sum_{i}^{N_{\mathrm{r}}} K_i \tag{12}$$

$$\sigma\,(K) = \frac{1}{N_{\mathrm{r}} - 1} \sqrt{\sum_{i}^{N_{\mathrm{r}}} (K_i - \langle K \rangle)^2}, \tag{13}$$

where $\langle\,\rangle$ denotes ensemble-averaging and N_{r} is the ensemble size ($N_{\mathrm{r}} = 20$ in this study; Table 2). The ensemble-averaged mean minimum inter-fiber spacing $\langle \bar{\delta}_1 \rangle$ was calculated in the same manner. The average permeability, as defined in Eq. 12, is known to be affected by the RVE size through its influence on fiber statistics and the influence of the boundary conditions on the computed flux. In principle, when the RVE size is sufficiently large or, under the assumption of ergodicity, when a sufficiently large ensemble size is used for relatively small RVEs, a correct or, convergent, mean behavior will be obtained, and the computed average permeability becomes the effective property. To determine the appropriate RVE size for a finite ensemble size, say $N_{\mathrm{r}} = 20$, computations were carried out on RVEs containing different numbers of fibers ($16 < N_{\mathrm{f}} < 600$), which were generated with $\delta_{\min} = 0.1R$ at $\phi = 0.45, 0.55, 0.70$. The results are given in Fig. 4. A size effect is clear in these results as the computed average, $\langle K \rangle / R^2$, is observed to vary with the RVE size. It is also notable that the sample standard deviation is affected significantly by the RVE size. For $N_{\mathrm{r}} = 20$ realizations of small RVEs ($N_{\mathrm{f}} = 16$) with $\phi = 0.70$, the averaged permeability ($\langle K \rangle / R^2 = 0.105$) and the associated standard deviation ($\sigma(K) = 0.07$) are comparable to those reported in Sangani and Yao (1988) while the mean-normalized standard deviation is about five times smaller than that reported in Ghaddar (1995). At $\mathrm{N_f} > 100$, $\langle K \rangle / R^2$ seems to reach a plateau. This suggests that the size effect diminishes with an increase in RVE size, as expected. Based on these observations, an RVE size of $N_{\mathrm{f}} = 576$ and a ensemble size of $N_{\mathrm{r}} = 20$ were chosen in this study.

4.2 Comparison with earlier results

Simulations were carried out in the porosity range $0.45 < \phi < 0.90$ and $\delta_{\min}/R$ between 0.1 and 1.5, depending on ϕ. The conditions are summarized in Table 2. The obtained permeability results are compared to earlier theoretical as well as to selected experimental data for unidirectional fiber arrays. It should be pointed out that earlier results

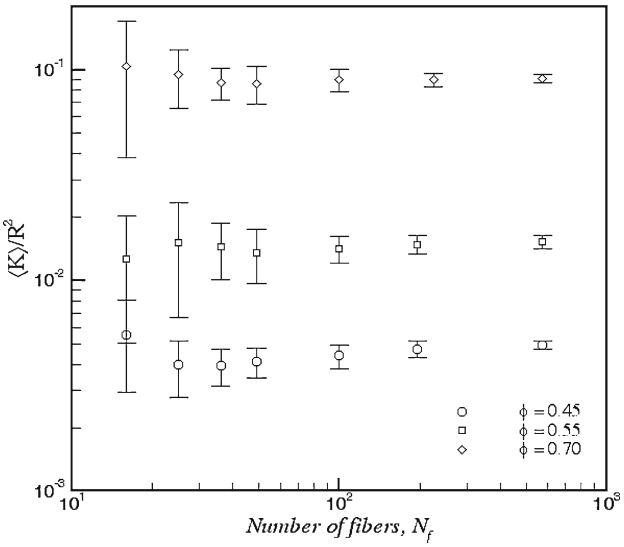

Fig. 4 RVE size effect on the averaged permeability. The circles, squares, and diamonds represent the ensemble-average permeability, averaged over 20 realizations of fiber distributions which were generated with $\delta_{\min} = 0.1R$ at $\phi = 0.45, 0.55, 0.70$, respectively. The error bars indicate the standard deviations $\pm\sigma(K)$

Table 3 Comparison of our results for the dimensionless permeability of random fiber arrays at various levels of porosity and $(\delta_{\min}/R)$—last three columns—with the results of Sangani and Yao (1988). The extent of microstructural variation at each porosity level was not examined in Sangani and Yao (1988), so a more direct comparison is not possible

Porosity	Sangani and Yao (1988)	$\delta_{\min}/R = 0.1$	$\delta_{\min}/R = 0.2$	$\delta_{\min}/R = 0.4$
0.9	1.67 ± 0.12	1.64 ± 0.06	1.63 ± 0.06	1.57 ± 0.06
0.7	0.102 ± 0.008	0.091 ± 0.004	0.092 ± 0.002	0.93 ± 0.002
0.5	0.0094 ± 0.0017	0.0084 ± 0.00045	0.0099 ± 0.00034	0.013 ± 0.00017

have not identified microstructure as a pertinent parameter and thus, the comparisons presented here are made with only ϕ as a parameter. In Fig. 5, our results at each porosity level are obtained for a range of the microstructural parameter $(\delta_{\min}/R)$, whose relation with K/R^2 will become clear latter in the manuscript. Here these results are compared to theoretical predictions for periodic (square and hexagonal) and random arrays and earlier results. In the range $0.765 < \phi < 0.90$, the permeability results of this work are in good agreement with the predictions of Sangani and Yao (1988) as well as of Spielman and Goren (1968). When $\phi < 0.7$, our results are in good agreement with Sangani and Yao (1988), while Spielman and Goren (1968) predicts an unrealistic flow blockage below $\phi \sim 0.6$. A more detailed comparison of our results to those of Sangani and Yao (1988) is given in Table 3.

In Fig. 6, permeability results are presented in terms of the Kozeny constant, k_c, defined as $k_c = \frac{\phi m^2}{K}$, where m is the mean hydraulic diameter of the porous medium. For visual clarity, only the mean values of our results are shown in that figure. Typically, k_c is only constant in a very narrow range of porosity. For random arrays,

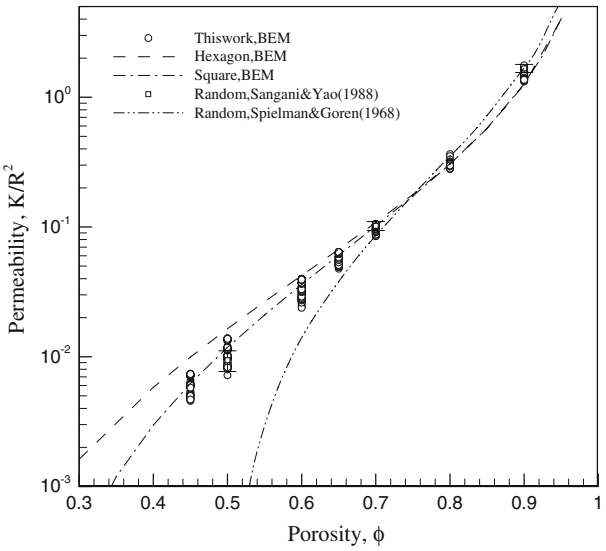

Fig. 5 Comparison of this work with earlier computational and theoretical results

k_c, as predicted by Spielman and Goren (1968), is about 9–10 for $0.75 < \phi < 0.85$. Its mean value at $\phi = 0.70$ is around 9.34 as predicted by Sangani and Yao (1988). Evidently, k_c is not a constant but varies with microstructure at any given porosity level. Our results indicate that k_c varies from 8 to 16 in the range $0.45 \leq \phi \leq 0.90$. At low porosities and in fiber systems of relevance to composites manufacturing, experimental data for k_c (Lam and Kardos 1991; Gutowski et al. 1987) show a scatter that is very similar to the scatter of our BEM results, in general extending above the predictions of regular arrays. It is interesting to notice that in the mid-to-low porosity range ($0.45 \leq \phi \leq 0.70$) the permeability behavior is not limited by the theoretical results for the square array. Indeed, all our BEM results, the earlier numerical results of Sangani and Yao (1988) as well as experimental data (Lam and Kardos 1991; Gutowski et al. 1987) show that the permeability of random arrays can fall below (or, equivalently, k_c can lie above) that of a square array. At high porosities ($\phi \sim 0.8$–0.9) the opposite is true; however, we believe this is due to the fact that at these high porosity levels fiber clustering occurs, rendering the systems more permeable. Unfortunately the definition of a random fiber array is ambiguous in earlier literature. To capture the permeability behavior in such arrays more precisely, additional microstructure details have to be taken into account.

4.3 Correlation between K and $\bar{\delta}_1$

Figure 7 shows two representative flow fields computed for unit cells containing 576 fibers at $\phi = 0.70$. The difference between the two fiber distributions lies in the choice of $\delta_{\min}$ ($\delta_{\min} = 0.1R$ in Fig. 7(a) and $\delta_{\min} = 1.0R$ in Fig. 7(b)) and the resulting statistics of δ_1. The flow contours show fluid speed at gray scales. From these two numerical examples, we see clearly how drastically the microstructure affects the distribution of flow in the interstitial space. A larger degree of local heterogeneity (caused by a smaller value of $\delta_{\min}$ and the resulting statistics of δ_1, for example Fig. 2) results in a broader distribution of fluid speeds. In this case, the fluid is stagnant between

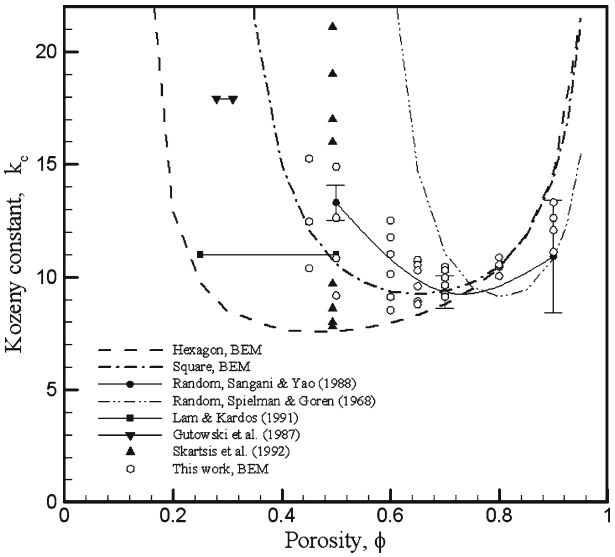

Fig. 6 Comparison of this work with related computational and experimental data in terms of the Kozeny constant

fiber aggregations or within closed rings of fibers, while a few major flow paths with relatively high flow speed exist. In the case of $\delta_{\min} = 1.0R$ a larger number of smaller flow paths form and the fluid speed is more uniform.

It is evident from Fig. 7 that fiber arrays of the same porosity can exhibit drastically different patterns of interstitial flow. It follows that the use of porosity alone cannot be expected to uniquely define their permeability. It also indicates that the reasons for the observed scatter in the latter, whether calculated numerically or determined by experiment, is to be sought in the underlying microstructure. In Fig. 8, the numerically computed $\langle K \rangle$ at each porosity level are plotted against $\langle \bar{\delta}_1 \rangle / R$. In this figure, the starting point of each curve is the permeability of the hexagonal array (filled square), for which the inter-fiber spacing is uniquely connected to porosity. From this plot, a distinct correlation between $\langle K \rangle / R^2$ and $\langle \bar{\delta}_1 \rangle / R$ is evident. In the range $0.45 < \phi < 0.7$ decreasing $\bar{\delta}_1$ or, equivalently, moving from a uniform array to arrays showing progressively higher degree of disorder, results in a permeability reduction. This trend is more pronounced at lower porosities ($\phi = 0.45, 0.5$). A similar permeability reduction as a result of non-uniformity in fiber distribution (quantified by the Morishita index in that case) was also reported in Bechtold and Ye (2003). This correlation can be qualitatively explained by the fact that, in the absence of large-scale clustering, the dominant flow resistance around each fiber is primarily caused by the narrowest gap formed between this fiber and its neighbors. In disordered fiber arrays the presence of narrow gaps has the effect of either deflecting a flow path, or reducing the corresponding flow rate. In both ways, narrower gaps will reduce the permeability. Figure 8 also shows the predictions of the lubrication model of Lundstrom and Gebart (1995) for regular arrays in which the inter-fiber spacing is modified by changing the fiber size while maintaining the porosity constant (see Appendix 1 below). It is clear that while Lundstrom and Gebart (1995) predicts the same qualitative features of the K vs. δ_1 behavior (a reduction of K with decreasing δ_1, the effect becoming more

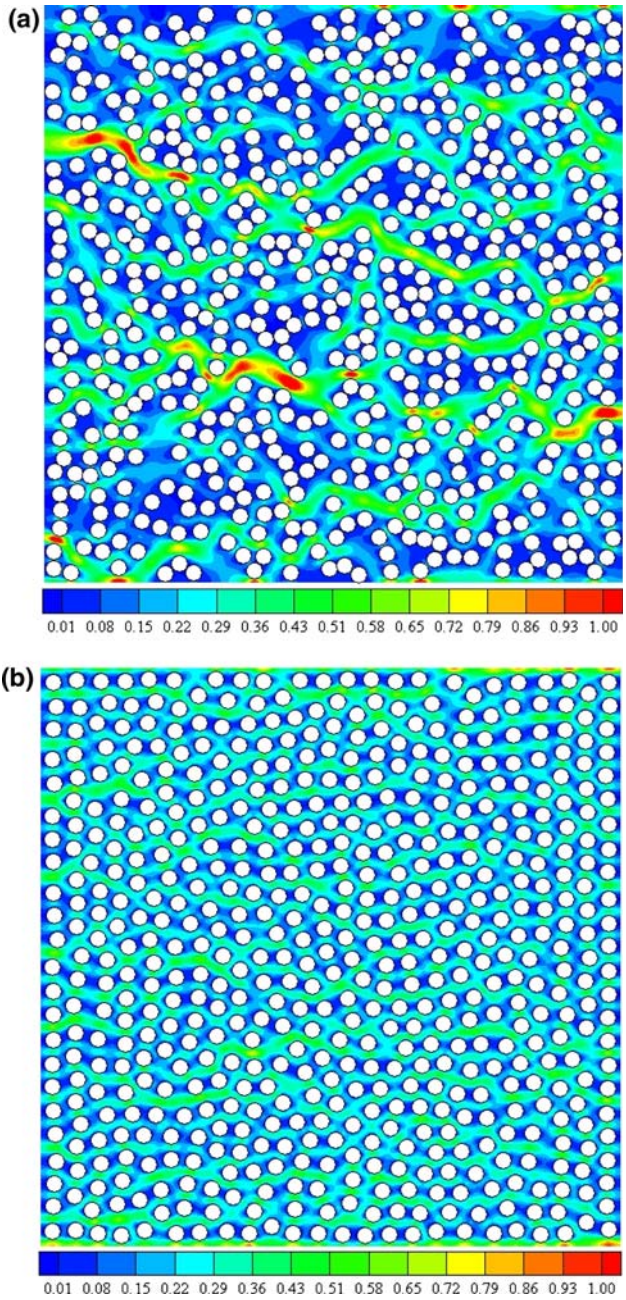

Fig. 7 Contours of fluid speed for transverse flows across unidirectional random fiber arrays: (**a**) $\phi = 0.7, \delta_{\min} = 0.1R, K/R^2 = 9.427 \times 10^{-2}$. (**b**) $\phi = 0.7, \delta_{\min} = 1.0R, K/R^2 = 1.024 \times 10^{-1}$

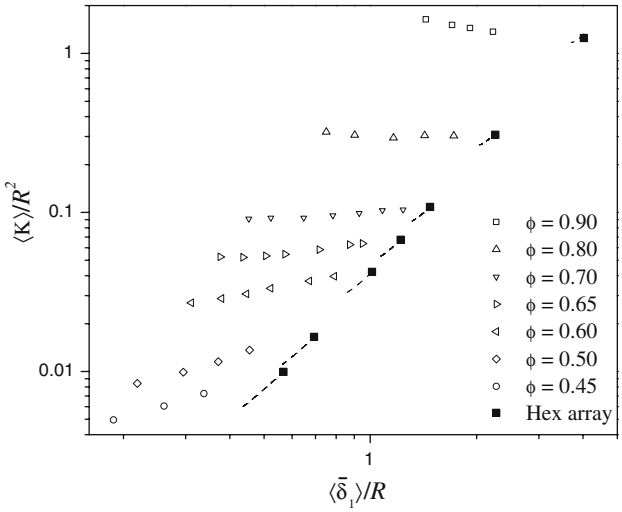

Fig. 8 Correlation of the normalized ensemble-averaged permeability ($\langle K \rangle / R^2$) with the ensemble-averaged mean nearest inter-fiber spacing $\langle \bar{\delta}_1 \rangle / R$. Also shown are permeability values for hexagonal arrays as well as the predictions of the lubrication model of Lundstrom and Gebart (1995)—broken line

pronounced as the porosity decreases), there are significant quantitative differences between the lubrication model and the computational results. Specifically, the attainable range of δ_1 at each porosity is smaller in Lundstrom and Gebart (1995) as required by the need to justify use of the lubrication approximation. In addition, our computational results fall consistently above the predictions of the lubrication theory. This is not surprising, since the flow in Lundstrom and Gebart (1995) is restricted to one unit cell, while in our computational models complex two-dimensional flow networks form (Fig. 7). In such 2D flow networks, the relative influence of small gaps on permeability is reduced, as flow is deflected to adjoining flow paths. Obviously, no such deflection is possible in a single unit-cell model. The predicted reduction in permeability caused by non-uniformity in fiber distribution is quite substantial. Comparing the curves corresponding to $\phi = 0.45$ and $\phi = 0.5$ in Fig. 8, it can be seen that the permeability of an array with $\phi = 0.5$ and $\left\langle \bar{\delta}_1 \right\rangle / R = 0.17$ is *lower* than the permeability of a hexagonal array at $\phi = 0.45$. Care should therefore be exercised when permeability models for regular arrays (for example Gebart (1992), Drummond and Tahir (1984), Bruschke and Advani (1993), Spielman and Goren (1968)) are used to derive estimates for the permeability of realistic and thus non-uniform arrays of fibers. At $\phi > 0.7$ an opposite trend is shown; this is probably due to the formation, at these high porosities, of flow channels whose size is comparable to the size of fiber aggregates.

In the porosity range of interest to composites manufacturing ($0.45 \leq \phi \leq 0.70$), Fig. 8 as well as the dependence between K and δ_1 suggested by Lundstrom and Gebart (1995) indicate that a functional form describing the relation between $\left\langle \bar{\delta}_1 \right\rangle$ and $\langle K \rangle$ should be:

$$\frac{\langle K\rangle}{R^2} = \left(\frac{\langle\bar{\delta}_1\rangle}{R}\right)^n f(\phi)\,, \tag{14}$$

where the exponent n is in general a function of porosity as indicated by the varying slopes of the data sets $\langle K\rangle$ vs. $\langle\bar{\delta}_1\rangle$ corresponding to different (ϕ) in Fig. 8. In seeking a functional form for $f(\phi)$, we recall that Eq. 14 should reduce to existing models for K when the fiber array becomes uniform. When the array approaches a uniform hexagonal array, $\bar{\delta}_1$ should equal the inter-fiber spacing of a hexagonal array $[\delta_{\text{hex}}/R = 2(\sqrt{\pi/2\sqrt{3}(1-\phi)} - 1)]$ and the corresponding dimensionless permeability will be $\frac{K_{\text{hex}}}{R^2} = \frac{\sqrt{3}}{3}\frac{16}{9\pi\sqrt{2}}(\frac{\delta_{\text{hex}}}{2R})^{2.5}$, both of which are functions of porosity only. To be asymptotically correct, the form of $f(\phi)$ should therefore be:

$$f(\phi) = \left(\frac{R}{\delta_{\text{hex}}}\right)^n \frac{K_{\text{hex}}}{R^2} \tag{15}$$

and thus Eq. 14 yields:

$$\frac{\langle K\rangle}{K_{\text{hex}}} = \left(\frac{\langle\bar{\delta}_1\rangle}{\delta_{hex}}\right)^n. \tag{16}$$

The exponent n is determined by fitting the computational results at each porosity according to Eq. 16. This gives the lowest estimate of n as $n = 0.164$ at $\phi = 0.7$ and the highest estimate $n = 0.628$ at $\phi = 0.45$. A plot of n vs. ϕ suggests a linear relationship $n = \alpha + \beta\phi$ with $\alpha = 1.51 \pm 0.06$ and $\beta = -1.93 \pm 0.10$. Analysis of the predictions of Lundstrom and Gebart (1995) (Appendix 1) in the same manner, also results in a linear relation between n and ϕ. Overall, a correlation between $\langle\bar{\delta}_1\rangle$ and $\langle K\rangle$ for random fiber arrays can be written as:

$$\frac{\langle K\rangle}{K_{\text{hex}}} = \left(\frac{\langle\bar{\delta}_1\rangle}{\delta_{\text{hex}}}\right)^{\alpha+\beta\phi}. \tag{17}$$

Taking logarithms in both sides of Eq. 17 results in:

$$\ln\left(\langle K\rangle/K_{\text{hex}}\right) = n(\phi)\ln\left(\langle\bar{\delta}_1\rangle/\delta_{\text{hex}}\right). \tag{18}$$

In Fig. 9 the permeability data are scaled and plotted as suggested by Eq. 18. The permeability corresponding to hexagonal arrays can be found at the top-right corner of the graph (coordinates (0,0)). The predictions of Lundstrom and Gebart (1995), scaled as indicated by Eq. 18, are also shown. Figure 9 tells us that as a fiber distribution changes from ordered to disordered, $\langle K\rangle$ will deviate from the permeability of hexagonal arrays along the path defined by Eq. 18. The corresponding least-square fit indicates a slope around one (0.994 ± 0.018) and an intercept very close to zero (-0.008 ± 0.01), as anticipated from Eq. 18.

5 Summary

We carried out an extensive investigation of Stokes flow across unidirectional disordered fiber arrays. The RVEs that are representative of these arrays were constructed

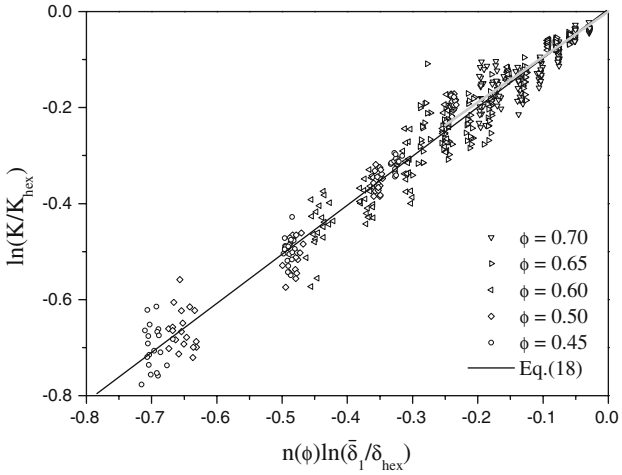

Fig. 9 A master curve, expressing the correlation between permeability and the mean nearest inter-fiber spacing in the porosity range $0.45 \leq \phi \leq 0.70$, plotted as $\ln\left(K/K_{\text{hex}}\right)$ vs. $n(\phi)\ln\left(\bar{\delta}_1/\delta_{\text{hex}}\right)$. The predictions of the model of Lundstrom and Gebart (1995) for perturbed hexagonal arrays are shown as a thick gray line on the top-right corner of the graph

using a Monte Carlo procedure in the porosity range $0.45 \leq \phi \leq 0.90$, each consisting of 576 fibers. With 20 realizations at each point in (δ_1, ϕ) space, a total of 620 simulations were carried out. This computationally intensive task was accomplished by developing and running an in-house parallel Boundary Element code on distributed memory parallel computers. Our results were compared to existing theoretical, numerical, and experimental results. Following this, we point out the need to consider some measure of the underlying fiber spatial statistics as an additional parameter affecting permeability. The microstructural characteristics of the model fiber distributions were analyzed and the mean nearest inter-fiber spacing $\bar{\delta}_1$ was identified as a parameter that correlates with the numerical estimates of K. Specifically, we found that, in the range of porosity studied, K is a statistical function of $\bar{\delta}_1$, with its average behavior $\langle K \rangle$ expressed by $\ln\left(\langle K \rangle / K_{\text{hex}}\right)/n = \ln\left(\left\langle \bar{\delta}_1 \right\rangle / \delta_{\text{hex}}\right)$, where (n) is a linear function of porosity and K_{hex} and δ_{hex} are also known functions of porosity. The deviation of (K) from this average behavior is related to the variability of the underlying microstructure, as expressed by the variance of δ_1.

Acknowledgements This work is supported by NSF Award No.DMI-0522221 and by the US Department of Energy, Office of Freedom CAR and Vehicle Technologies, Lightweight Materials Program. The authors also wish to thank the Albuquerque High Performance Computing Center for providing access to their IBM Netfinity 4500R Linux cluster on which the parallel computations reported in this study were carried out.

Appendix 1

Lundstrom and Gebart (1995) studied, in the context of the lubrication approximation, the effect of perturbation of fiber radii as well as perturbation of fiber positions on the transverse permeability of ordered unidirectional fiber arrays. In the case of

direct relevance to this study, perturbed arrays were generated from regular hexagonal ones, whose fibers' size was allowed to vary in a regular manner while the total volume fraction remained constant. A hexagonal array of fibers of radius (R) is thus replaced by a sequence of alternating "larger" and "smaller" fibers, whose radii are $(R+\varepsilon)$ and $(R-\varepsilon)$, respectively. The porosity is held constant by changing the unit-cell dimensions in order to accommodate the changed fiber radii. It is noted that in this case there are two inter-fiber gap widths; one forms between large and adjacent small fibers and is denoted as δ_1 while the other forms between adjacent small fibers and is $\delta_2 = \delta_1 + 2\varepsilon$. The expression for the narrower gap δ_1 in terms of porosity ϕ and the size parameter $\varepsilon_m(\varepsilon_m = \varepsilon/R)$ is:

$$\frac{\delta_1}{R} = \frac{2}{\sqrt{3}}\sqrt{\frac{\pi\left[(1-\varepsilon_{\mathrm{m}})^2 + \frac{1}{2}(1+\varepsilon_{\mathrm{m}})^2\right]}{\sqrt{3}(1-\phi)}} - 2. \tag{A1}$$

In the range of small $\varepsilon_{\mathrm{m}}(\varepsilon_{\mathrm{m}} < 0.35)$ Eq. A1 shows a monotonic behavior; as ε_{m} increases, δ_1 decreases. The transverse permeability K' of the resulting fiber array is:

$$\frac{K'}{R^2} = \frac{16\sqrt{3}}{9\pi\sqrt{2}} \cdot \left[2\sqrt{1-\varepsilon_{\mathrm{m}}^2} + \sqrt{\frac{[1-\varepsilon_{\mathrm{m}}]\delta_1}{\delta_1 + 2\varepsilon}}\right]^{-1} \cdot \left(\frac{\delta_1}{2R}\right)^{5/2}. \tag{A2}$$

The behavior of K' mirrors the trend shown in Eq. A1 for the minimum inter-fiber spacing δ_1. The predictions of Eqs. A1, A2 for $\varepsilon/R < 0.35$ are shown in Fig. 8. The predictions of Eq. A2 are also plotted as suggested by Eq. 16 and the corresponding exponent (n) is calculated. This is found to be linearly dependent on porosity. Following this, the predictions of Eqs. A1, A2 are scaled as suggested by Eq. 18 and plotted along with our computational results in Fig. 9.

References

Astrom, B.T., Pipes, R.B., Advani, S.G.: On flow through aligned fiber beds and its applications to composites processing. J. Compos. Mater. **26**(9), 1351–1373 (1992)

Bechtold, G., Ye, L.: Influence of fibre distribution on the transverse flow permeability in fibre bundles. Compos. Sci. Technol. **63**, 2069–2079 (2003)

Beer, G.: Programming the Boundary Element Method. John Wiley & Sons, New York (2001)

Blackford, L.S., Choi, J., Cleary, A., D'Azevedo, E., Demmel, J., Dhilllon, I., Dongarra, J., Hammarling, S., Henry, G., Stanley, K., Walker, D., Whaley, R.C.: ScaLAPACK User's Guide. SIAM, Philadelphia (1997)

Bruschke, M.V., Advani, S.G.: Flow of generalized Newtonian fluids across a periodic array of cylinders. J. Rheol. **37**(3), 479–498 (1993)

Cai, Z., Berdichevsky, A.L.: Numerical-simulation on the permeability variations of a fiber assembly. Polym. Compos. **14**, 529–539 (1993)

Diggle, P.J.: Statistical Analysis of Spatial Point Patterns, 2nd edn. Oxford University Press, Oxford (2003)

Drummond, J.E., Tahir, M.I.: Laminar viscous flow through regular arrays of parallel solid cylinders. Int. J. Multiphase Flow **10**(5), 515–540 (1984)

Ferland, P., Guittard, D., Trochu, F.: Concurrent methods for permeability measurement in resin transfer molding. Polym. Compos. **17**(1), 149–158 (1996)

Gao, X., Davies, T.G.: Boundary Element Programming in Mechanics. Cambridge University Press, Cambridge (2002)

Gebart, B.R.: Permeability of unidirectional reinforcements for RTM. J. Compos. Mater. **26**(8), 1100–1133 (1992)

Gebart, B.R., Lidstrom, P.: Measurement of inplane permeability of anisotropic fiber reinforcements. Polym. Compos. **17**(1), 43–51 (1996)

Ghaddar, C.K.: On the permeability of unidirectional fibrous media: a parallel computational approach. Phys. Fluids **7**(11), 2563–2586 (1995)
Gropp, W., Lusk, E.: Using MPI: Portable Parallel Programming with the Message Passing Interface. MIT Press, Cambridge (1994)
Gutowski, T.G., Cai, Z., Bauer, S., Boucher, D.: Consolidation experiments for laminate composites. J. Compos. Mater. **21**, 650–669 (1987)
Happel, J.: Viscous flow relative to arrays of cylinders. AIChE J. **5**(2), 174–177 (1959)
Hasimoto, H.: On the periodic fundamental solutions of the Stokes equations and their applications to viscous flow past a cubic array of cylinders. J. Fluid Mech. **5**(2), 317–328 (1959)
Howells, I.D.: Drag due to the motion of a Newtonian fluid through a sparse random array of small fixed rigid objects. J. Fluid. Mech. **64**, 449–475 (1974)
Keller, J.B.: Viscous flow through a grating or lattice of cylinders. J. Fluid. Mech. **18**(1), 94–96 (1964)
Koch, D.L., Brady, J.F.: The effective diffusivity of fibrous media. AIChE J. **32**(4), 575–591 (1986)
Lam, R.C., Kardos, J.L.: The permeability and compressibility of aligned and cross-plied carbon fiber beds during processing of composites. Polym. Eng. Sci. **31**, 1064–1069 (1991)
Loendersloot, R., Akkerman, R., Lomov, S.V. : A permeability prediction for un-sheared non-crimp fabrics. In: Advani, S. (ed.) Seventh International Conference on Flow Processes in Composite Materials, pp. 1064. University of Delaware, Newark (2004)
Lundstrom, T.S., Gebart, B.R.: Effect of perturbation of fiber architecture on permeability inside fiber tows. J. Compos. Mater. **29**(4), 424–443 (1995)
Lundstrom, T.S., Gebart, B.R., Sandlund, E.: In-plane permeability measurements on fiber reinforcements by the multi-cavity parallel flow technique. Polym. Compos. **20**(1), 146–154 (1999)
Ngo, N.D., Tamma, K.K.: Complex three-dimensional microstructural permeability prediction of porous fibrous media with and without compaction. Int. J. Num. Meth. Eng. **60**, 1741–1757 (2004)
Nordlund, M., Lundstrom, T.S., Frishfelds, V., Jacovics, A.: Permeability network model for non-crimp fabrics. Composites Part A **37**, 826–835 (2006)
Papathanasiou, T.D.: The hydraulic permeability of periodic arrays of cylinders of varying size. J. Porous Media **4**(4), 323–336 (2001)
Papathanasiou, T.D., Lee, P.D.: Morphological effects on the transverse permeability of arrays of aligned fibers. Polym. Compos. **18**(2), 242–253 (1997)
Parnas, R.S., Flynn, K.M., Dal-Favero, M.E.: A permeability database for composite manufacturing. Polym. Compos. **18**(5), 623–633 (1997)
Pozridikis, C.: Boundary Integral and Singularity Methods for Linearized Viscous Flow. Cambridge University Press, Cambridge (1992)
Pyrz, R.: Quantitative description of the microstructure of composites. Part I: Morphology of unidirectional composite systems. Compos. Sci. Technol. **50**, 197–208 (1994)
Ripley, B.: Spatial Statistics. Wiley, New York (1981)
Sangani, A.S., Acrivos, A.: Slow flow past periodic arrays of cylinders with application to heat transfer. Int. J. Multiphase Flow **8**, 193–201 (1982)
Sangani, A.S., Yao, C.: Transport processes in random arrays of cylinders. II. Viscous flow. Phys. Fluids **31**(9), 2435–2444 (1988)
Skartsis, L., Kardos, J.L., Khomami, B.: Resin flow through fiber beds during composite manufacturing processes Part I: Review of Newtonian flow through fiber beds. Polym. Eng. Sci. **32**(4), 221–230 (1992a)
Skartsis, L., Khomami, B., Kardos, J.L.: Resin flow through fiber beds during composite manufacturing processes. Part II: Numerical and experimental studies of Newtonian flow through ideal and actual fiber beds. Polym. Eng. Sci. **32**(4), 231–239 (1992b)
Song, Y.S., Chung, K., Kang, T.J., Youn, J.R.: Prediction of permeability tensor for three dimensional circular braided preform by applying a finite volume method to a unit cell. Comp. Sci. Tech. **64**, 1629–1636 (2004)
Spielman, L., Goren, S.L.: Model for predicting pressure drop and filtration efficiency in fibrous media. Environ. Sci. Technol. **2**, 279–287 (1968)
Torquato, S.: Random Heterogeneous Materials, 1st edn. Springer-Verlag, New York (2002)
Weitzenbock, J.R., Shenoi, R.A., Wilson, P.A.: Radial flow permeability measurement. Part A: Theory. Composites Part A **30**(6), 781–796 (1999)
Yu, B., Lee, J., Cao, H.: A fractal in-plane permeability model for fabrics. Polym. Comp. **23**(2), 201–221 (2002)